

# Computational Study on the Cardiovascular System: Ventricular–Ventricular Interaction and Right Ventricular Failure in Pulmonary Arterial Hypertension

Tammo Delhaas, Theo Arts, Yvette Koeken,  
Joost Lumens, Georgina Palau-Caballero,  
and John Walmsley

## Abstract

In this chapter, we describe how the CircAdapt model of the heart and circulation has been used to both increase our understanding of the pathophysiology of pulmonary arterial hypertension (PAH) and predict the effects of therapy. Simulation results reproduce key features of mechanical incoordination observed in PAH patients, including early diastolic septal motion and strain abnormalities. Our simulations suggest that septal movement is not dependent solely on the transeptal pressure gradient. Additionally, an imbalance of forces at the right ventricular (RV) attachment points resulting from ongoing RV free wall contraction during the early diastolic phase causes abnormal septal motion. We also demonstrate that atrial septostomy in patients with severe PAH might be beneficial because it increases left ventricular (LV) preload and, consequently, allows better maintenance of systemic arterial blood pressure during exercise. Finally, we show that pacing the RV free wall in severely decompensated PAH results in more synchronous LV and RV pressure decay, more homogeneous distribution of myofiber load over the ventricular walls, and a slight improvement of RV pump function.

---

T. Delhaas (✉) • T. Arts • Y. Koeken • J. Lumens  
G. Palau-Caballero • J. Walmsley  
Department of Biomedical Engineering  
Cardiovascular Research Institute Maastricht  
(CARIM), Maastricht University Medical Center,  
Maastricht, The Netherlands  
e-mail: [tammo.delhaas@maastrichtuniversity.nl](mailto:tammo.delhaas@maastrichtuniversity.nl)

---

**Keywords**PAH • Computer model • Ventricular interaction • Hemodynamics  
Myocardial deformation • Circadapt • Right ventricular failure • Pacing

---

**Introduction**

A wealth of new information about the cardiovascular system in pulmonary arterial hypertension (PAH) has become available due to the technological advances in imaging over the past decades. Considerable insights into right ventricular (RV) function as well as the pathophysiology of PAH have been gained from echocardiography and cardiac magnetic resonance imaging [1, 2]. However, the challenge to interpret these imaging results increases proportionally with the amount of available information, especially in diseases with low prevalence, such as PAH [3]. Mechanistic mathematical modeling based on physics and physiology is a promising alternative approach to the study of physiological and pathophysiological responses in patients. In this chapter, we describe how the CircAdapt model of the heart and circulation has increased our understanding of the pathophysiology of PAH, and how we can use the model to assess the effect of therapy.

---

**The CircAdapt Model**

The CircAdapt model was developed in an attempt to reduce the input information required for computational models, and to focus on clinically measurable output data [4–7]. CircAdapt allows rapid simulation of cardiac pump function and cardiovascular system dynamics for both research and educational purposes ([www.circadapt.org](http://www.circadapt.org)). The model consists of a network composed of a limited number of module types, i.e., chambers, valves, tubes and resistances (Fig. 7.1a). The CircAdapt model generates tracings of hemodynamic and mechanical variables (such as cardiac and vascular pressures and volumes, flow through cardiac valves, and local tissue mechanics as a function of time over the

entire cardiac cycle. When using the educational version, simulation of a single cardiac beat in real-time, can be displayed on a regular PC.

The heart in the CircAdapt model consists of five walls, i.e., the left and right atrial walls, the left and right ventricular wall, and the interventricular septum. Cavity pressures are calculated from cavity volumes as follows. Cavity volumes determine wall area. Wall areas determine strain of the myofibers in the wall. A model of myofiber mechanics is used to calculate myofiber stress from myofiber strain. Myofiber stress then determines wall tension in each cardiac wall. The mechanical equilibrium between the three ventricular walls is used to calculate their shape when encapsulating the two ventricular cavities (Fig. 7.1b) via the TriSeg module [5]. Transmural pressure is calculated for each wall from wall tension and curvature using Laplace's law. Finally, cavity pressures are found by adding the transmural pressures to the intra-pericardial pressure surrounding the myocardial walls.

Non-linear elastic tube modules with characteristic impedance for pressure-flow waves represent large blood vessels (arteries and veins). Valves with inertia and Bernoulli pressure losses connect tubes and chambers. Effective orifice area of a cardiac valve depends on direction and magnitude of flow through the valve and on pressure drop over the valve. Non-linear resistances that connect the pulmonary and systemic arterial and venous tube modules represent the pulmonary and systemic vascular beds. Finally, a passive elastic sheet surrounding the entire heart (ventricles and atria) is included to represent the pericardium.

An important and unique feature of the CircAdapt model is that it reduces the number of independent parameters through implementation of structural adaptation of cardiac and vascular walls to mechanical load of the tissue. Size and mass of cardiac walls and large blood vessels

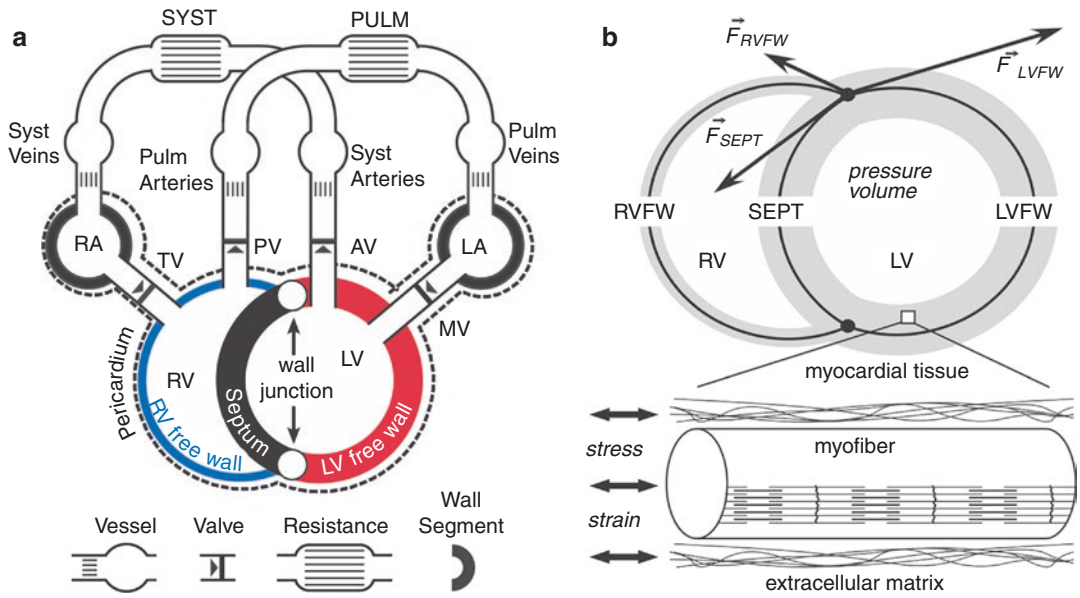


**Fig. 7.1** (a) The CircAdapt model. (b) The TriSeg module of ventricular mechanics. AV aortic valve,  $F$  force, LA left atrium, LV left ventricle, LVFW left ventricular free wall, MV mitral valve, Pulm pulmonary, PV pulmonary

valve, RA right atrium, RV right ventricle, RVFW right ventricular free wall, SEPT interventricular septum, Syst systemic, TV tricuspid valve

adapt to normalize local mechanical tissue load to tissue-specific physiological levels [4, 6].

### Suitability of the CircAdapt Model for Realistic Modeling of Pulmonary Arterial Hypertension

The multiscale nature of the CircAdapt model allows us to relate global pump mechanics of the cardiac chambers to both systemic hemodynamics and local mechanics of the myocardium. CircAdapt integrates basic physical and physiological principles such as conservation of energy. In the current context, this means that the total amount of contractile work generated by the myofibers should equal the total amount of hydraulic pump work as delivered by the ventricles. Importantly, the model also incorporates ventricular interaction through mutual mechanical and hemodynamic dependence of the LV and the RV. Hemodynamic interaction follows due to the series coupling within the pulmonary and the systemic circulations [8]. CircAdapt also predicts mechanical interaction via the interventricular

septum in which a change of shape, size or pressure-volume relation of one ventricle affects the shape, size and pressure-volume relation of the other ventricle through the septum [9]. The modular nature of the CircAdapt model allows us the versatility to introduce additional valves to represent (for example) an atrial septal defect. Finally, the relatively stiff pericardial sac surrounding the heart limits acute cardiac distension and, thereby, modulates mechanical ventricular interaction [10].

### Simulation of Normal Cardiovascular Mechanics and Hemodynamics

Normal left and right heart dynamics were simulated during rest and exercise (Fig. 7.2). The methods used to obtain these simulations have been published in detail elsewhere [5]. Major input parameter values were: mean systemic arterial blood pressure of 92 mmHg (rest and exercise), cardiac output 5.1 l/min (rest) and 15.3 l/min (exercise), and heart rate 70 beats/min (rest)

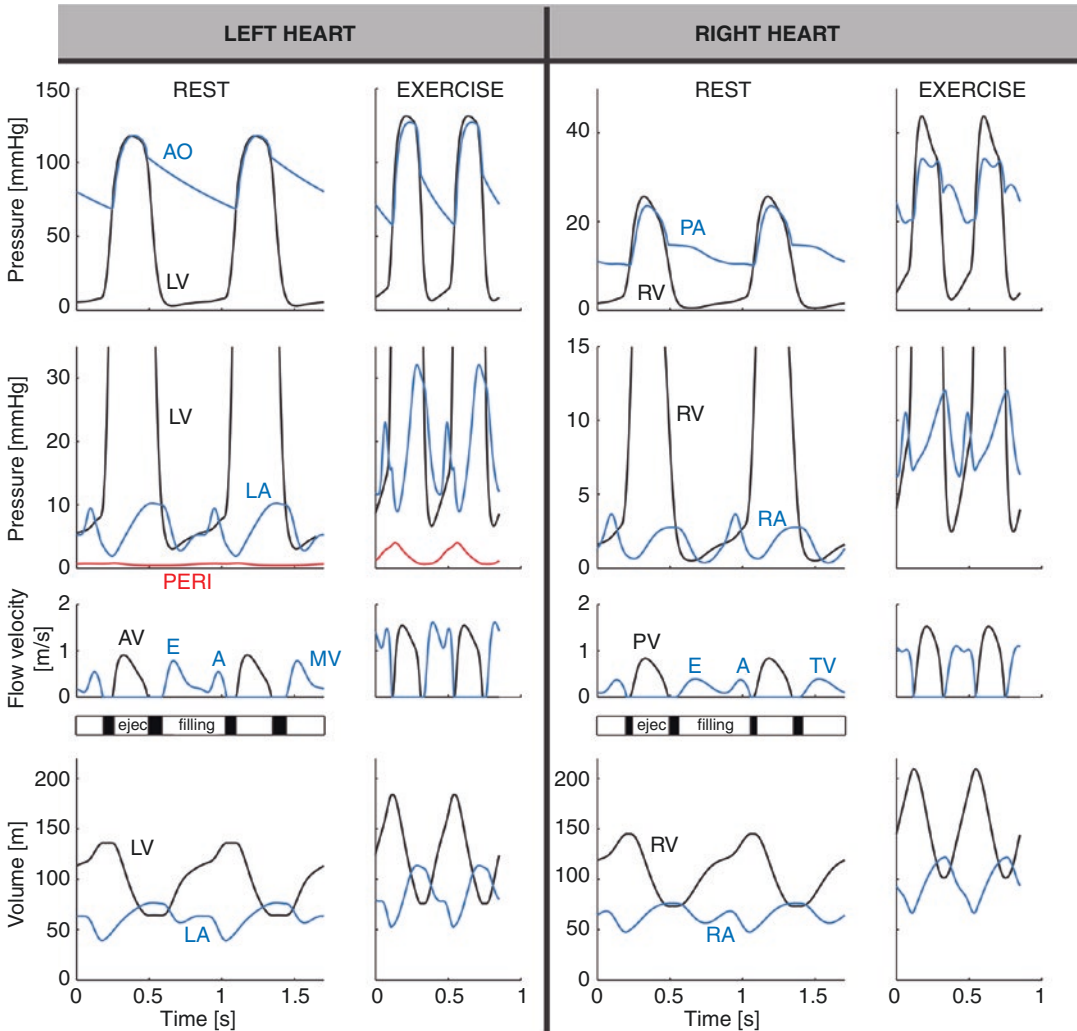


**Fig. 7.2** CircAdapt simulation of normal left and right heart dynamics at rest and during exercise. A atrial contraction-induced late filling wave, AV aortic valve, E early mitral filling wave, *ejec* ejection, LA left atrium, LV

left ventricle, MV mitral valve, *PERI* pericardial, PV pulmonary valve, RA right atrium, RV right ventricle, TV tricuspid valve

and 140 beats/min (exercise). Simulated time courses for pressure and volume were physiologic, both at rest and during exercise: time courses of mitral and tricuspid valve flows showed an early passive filling wave (E) followed by a clearly separated late filling wave (A) that resulted from atrial contraction; atrial contraction induced a rise in LV and RV cavity pressures and volumes towards the end of diastole; inertia effects can be appreciated from the negative pressure gradients across the AV-valves towards the

ends of both the E- and A-waves as well from the negative pressure gradient across the aortic and pulmonary valve towards end of the ejection phase; LV and RV end-diastolic volumes were not significantly different; opening of the pulmonary valve occurred earlier than the opening of the aortic valve, whereas its closure was later. The model appropriately simulated the effects of acute alterations in loading conditions that reflected the changes seen during exercise (Fig. 7.2, right panels).

## Developmental Stages of PAH

Development of PAH is characterized by progressive remodeling and vasoconstriction of the pulmonary vasculature leading to a gradual increase of pulmonary vascular resistance. RV pressure increases to maintain cardiac output and may finally approach or even exceed LV pressure. During the early stages of the disease, RV free wall mass increases (hypertrophy) to compensate for the increase in RV afterload and to decrease wall stress to within normal physiological ranges [11, 12]. As the disease progresses, RV free wall tissue can no longer adequately adapt to the increased load and, as a result, cardiac myocytes (and presumably also sarcomeres) become over-stretched [13], RV end-diastolic volume increases [14] and RV pump function deteriorates [15]. These morphological and functional changes will ultimately result in decompensated right heart failure, characterized by an increase in RV filling pressures, development of RV diastolic dysfunction, RV dilatation, and decreased cardiac output [16].

## CircAdapt Simulation Protocol for PAH

We took the different disease stages of PAH into account in the simulation protocol for the CircAdapt model. Starting from our baseline (NORMAL) simulation at rest, a first simulation of mild compensated PAH (PAH-Comp) was obtained by increasing pulmonary vascular resistance (PVR) while allowing the heart and large blood vessels to structurally adapt to normalize mechanical tissue load. This adaptation process resulted in an increase of the mean pulmonary artery pressure (mPAP) from 18 mmHg, in the NORMAL simulation, to 32 mmHg in the PAH-Comp simulation while RV free wall (RVFW) mass increased by 40% to normalize cardiac stresses and strains to tissue-specific physiological levels [4]. States of moderately and severely decompensated PAH (PAH-DecompMod and PAH-DecompSev, respectively) were achieved by increasing PVR so that mPAP was equal to 55

and 79 mmHg, respectively, while further adaptation of cardiac and vascular walls to mechanical load was prevented.

## Ventricular Hemodynamics and Mechanics in Simulated PAH

In the PAH-Comp simulation, the increase of PVR influenced neither the RV end diastolic volume (140 ml) nor the RV ejection fraction (52%). PAH-Decomp simulations showed increases of RV end-diastolic volume towards 169 and 217 ml for the moderately and severely decompensated PAH simulations, respectively. RV systolic pump function deteriorated as is evident from the decrease of RV ejection fraction to 43 and 33% for the moderate and severely decompensated PAH simulation, respectively.

Figure 7.3 shows changes in time courses of simulated ventricular pressures and circumferential strains from normal conditions to PAH-DecompSev. While RV pressures increased during the PAH simulations (Fig. 7.3: top panel row), it only exceeded LV pressure in the PAH-DecompSev simulation during diastole and late systole. When RV pressures were normalized to peak LV pressure (Fig. 7.3: middle panel row), it can be observed that PAH hardly affected the timing of LV pressure rise and decay; however, RV pressure decay was delayed proportionally to PAH severity. The LV-to-RV time difference in pressure decay changed from +28 ms in the NORMAL simulation to –40 ms in PAH-DecompSev. This delay in RV pressure decay was associated with delayed RV isovolumic relaxation as can be appreciated from the time courses of circumferential strains (Fig. 7.3, bottom panel row). Whereas in the NORMAL and PAH-Comp simulations the strain patterns were relatively synchronous and uniform in the three ventricular walls (Fig. 7.3: bottom panel row), in the simulations of decompensated PAH circumferential strain patterns changed. During isovolumic contraction, the initial shortening of the LVFW and SEPT caused a stretch of the RVFW. This stretch resulted in a delay in the onset of RVFW shortening compared with that of the

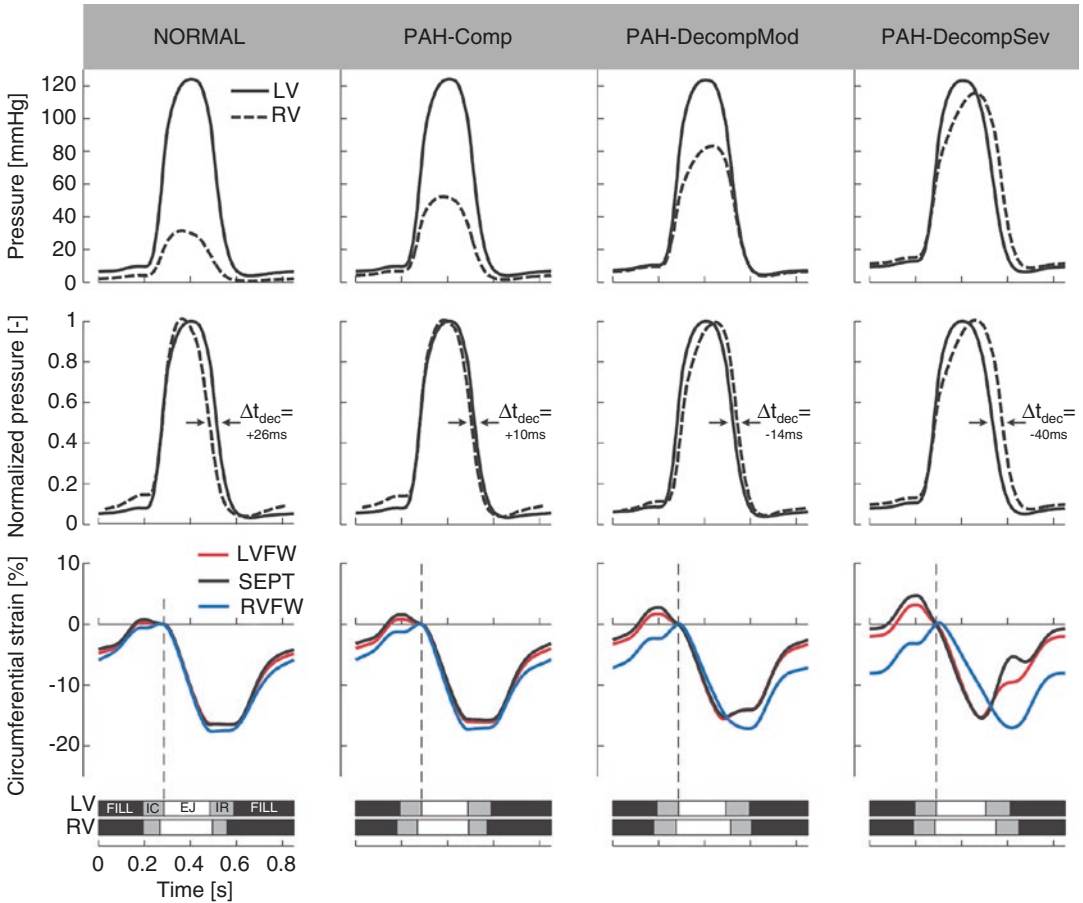


**Fig. 7.3** Time courses of simulated ventricular pressures and circumferential strains under normal and PAH conditions. *EJ* ejection phase, *Fill* filling phase, *IC* isovolumic contraction phase, *IR* isovolumic relaxation phase, *LV* left ventricle, *LVFW* left ventricular free wall, *NORMAL* normal ventricular loading conditions at rest, *PAH-Comp*

PAH loading conditions with compensation, *PAH-DecompMod* moderately decompensated PAH condition, *PAH-DecompSev* severely decompensated PAH condition, *RV* right ventricle, *RVFW* right ventricular free wall, *SEPT* interventricular septum,  $\Delta t_{dec}$  LV-to-RV time delay in pressure decay. Adapted from [32]

LVFW and SEPT as well as in an on-going RVFW shortening into the isovolumic relaxation phase with peak RVFW shortening occurring at the moment of mitral valve opening. Closure of the pulmonary valve was delayed concomitantly with PAH severity (Fig. 7.3, bars at bottom).

### Septal Movement in Simulated PAH

It is well established that septal position is related to transeptal pressure gradient [17]. Our model realistically reproduces the abnormal position and

motion pattern of the interventricular septum, which is one of the most characteristic phenomena seen in PAH patients [18]. Figure 7.4 shows tracings of septal curvature throughout the cardiac cycle. In the *NORMAL* simulation, septal wall curvature is always positive, indicating that the septum always bulges towards the RV. With increasing severity of PAH, hence with decreasing transeptal pressure gradient, septal wall curvature decreases, indicating flattening of the septal wall. In the moderately decompensated PAH simulation, the septal wall apparently decreases its curvature towards the end of the ejection phase and even

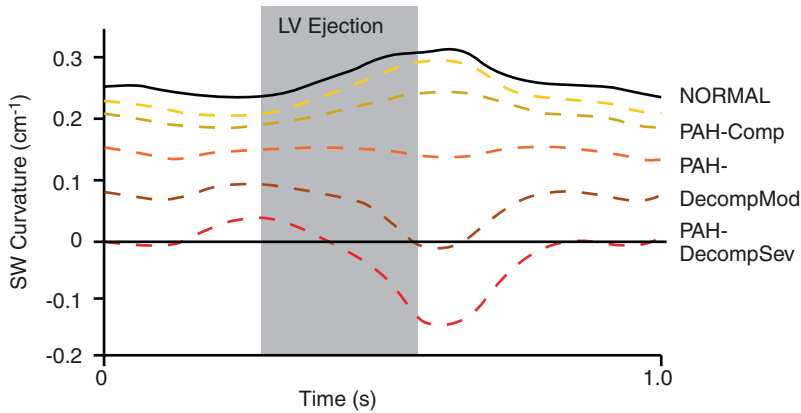


**Fig. 7.4** Time courses of septal wall curvature under normal and PAH conditions. *LV* left ventricular, *SW* septal wall, *NORMAL* normal ventricular loading conditions at rest, *PAH-Comp* PAH loading conditions with compensa-

tion, *PAH-DecompMod* moderately decompensated PAH condition, *PAH-DecompSev* severely decompensated PAH condition

bulges just towards the LV in early diastole. The septal wall flattening occurs despite the fact that in the *PAH-DecompMod* simulation LV pressure exceeded RV pressure throughout almost the entire cardiac cycle (see Fig. 7.3), indicating that transseptal pressure gradient does not entirely explain the motion of the septum. In the severely decompensated PAH simulation, the septum clearly bulges towards the LV from midway through the ejection phase until midway through diastole, corresponding with the fact that transseptal pressure gradient also changed direction during this part of the cardiac cycle.

Our results clearly show that septal movement is not dependent solely on the transseptal pressure gradient. We propose that an imbalance of forces at the RV attachment points resulting from ongoing RVFW contraction during the early diastolic phase pulls the septum leftwards, providing an additional source of septal movement.

### ***In Silico* Testing of Interventions in PAH**

These studies established that the *CircAdapt* model can produce realistic simulations of cardiac mechanics and hemodynamics under normal and PAH conditions. We therefore set out to use

the model to test several therapeutic interventions in PAH.

### **Atrial Septostomy in PAH**

To clarify whether the benefits of atrial septostomy (AS) in PAH patients are explained by increase of oxygen availability in the tissues, the possibility to maintain blood pressure during exercise, or a combination of these factors [19–21], we evaluated effects of AS using *CircAdapt* [22]. We assessed the immediate effects of a circular AS with diameters ranging from 1 to 16 mm for levels of PAH with mean pulmonary arterial pressure (mPAP) ranging from 50 to 82 mmHg. Mean systemic arterial pressure was set to 61 mmHg to mimic pediatric blood pressure levels. The top panel of Fig. 7.5 shows the ratio of pulmonary to systemic blood flow as a function of shunt size and mPAP. It shows that shunts with a diameter of 1 to 2 mm resulted in almost no flow across the shunt. For shunt sizes of 3 mm and more, the ratio of pulmonary blood flow to systemic blood flow ( $Q_p/Q_s$ ) was almost proportional to mPAP. The size and the direction of the shunt flow depended both on mPAP and shunt size. For shunt diameters above 2 mm,  $Q_p/Q_s$  was only proportional to the extent of pulmonary

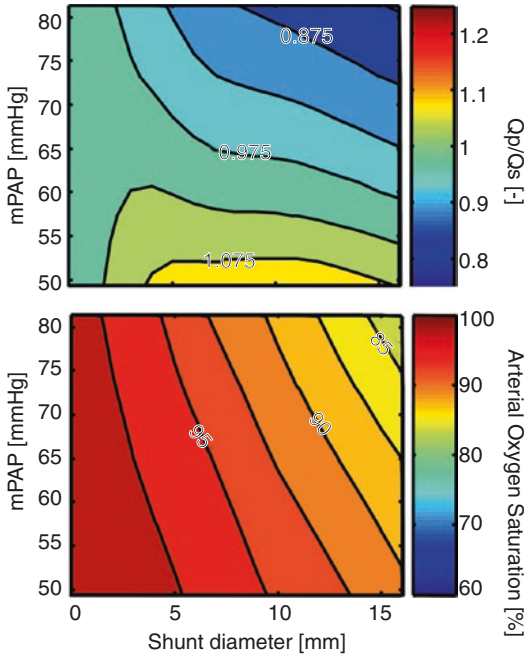


**Fig. 7.5** Blood flow distribution and arterial oxygen saturation as a function of PAH severity and atrial septal defect diameter. *ASD* atrial septal defect, *mPAP* mean pulmonary arterial pressure,  $Q_p$  pulmonary blood flow,  $Q_s$  systemic blood flow

hypertension. Atrial septostomy led to a decrease in both upper and lower body arterial oxygen saturation that was proportional to both *mPAP* and shunt size (Fig. 7.5, lower panel). Simulations of exercise with severe PAH showed that these PAH patients benefit from an ASD because right-to-left atrial shunt flow facilitates maintenance of systemic arterial pressure [22]. Systemic oxygen transport, defined as systemic flow multiplied by the systemic arterial oxygen saturation, increased with exercise because the decrease in arterial oxygen saturation is overcompensated for by the increase in flow [20, 23]. However, in the presence of a right-to-left shunt, desaturated blood will bypass the pulmonary vascular bed and, hence, systemic blood flow does not reflect effective pulmonary blood flow any more, but is the sum of the right-to-left shunt and the effective pulmonary blood flow. Therefore, effective systemic oxygen transport capacity, being the product of effective pulmonary blood flow and pulmonary venous saturation, does not increase

after atrial septostomy in PAH patients. We therefore believe that AS might be beneficial to patients with severe PAH because it increases LV preload and, consequently, allows better maintenance of systemic arterial blood pressure during exercise.

## RV Free Wall Pacing in PAH

Several studies have shown that morbidity and mortality of PAH patients are determined by the ability of the RV to maintain normal stroke volume and cardiac output [24, 25]. In PAH, structural remodeling (hypertrophy and dilatation) is limited to the RVFW [14], suggesting an inhomogeneous distribution of myocardial tissue load. Local reduction of mechanical load of the RVFW may therefore be another therapeutic option, in addition to conventional reduction of pulmonary vascular resistance [26].

Severe PAH patients have interventricular mechanical dyssynchrony with prolonged duration of shortening and delayed peak shortening in the RV free wall compared with that of the LV free wall and the interventricular septum [27, 28]. RVFW shortening continued even after pulmonary valve closure and appeared to relate to leftward septal motion during LV isovolumic relaxation. As a potential treatment, early RVFW pacing was suggested as a way to improve interventricular mechanical synchrony and, thereby, cardiac pump function [19, 28, 29]. In our opinion, RVFW pacing also seems logical because during ventricular pacing, mechanical myofiber work is significantly decreased in early-activated regions, whereas it is increased in late-activated regions [30, 31].

Using the CircAdapt model, we tested the hypothesis that early pacing of the RV free wall improves ventricular mechanical coordination and, thereby, global RV pump function in PAH [32]. Model simulations also showed interventricular mechanical dyssynchrony in severely decompensated PAH (Fig. 7.6). This mechanical dyssynchrony was associated with prolonged duration of RV free wall shortening and inhomogeneous distribution of myofiber load over the



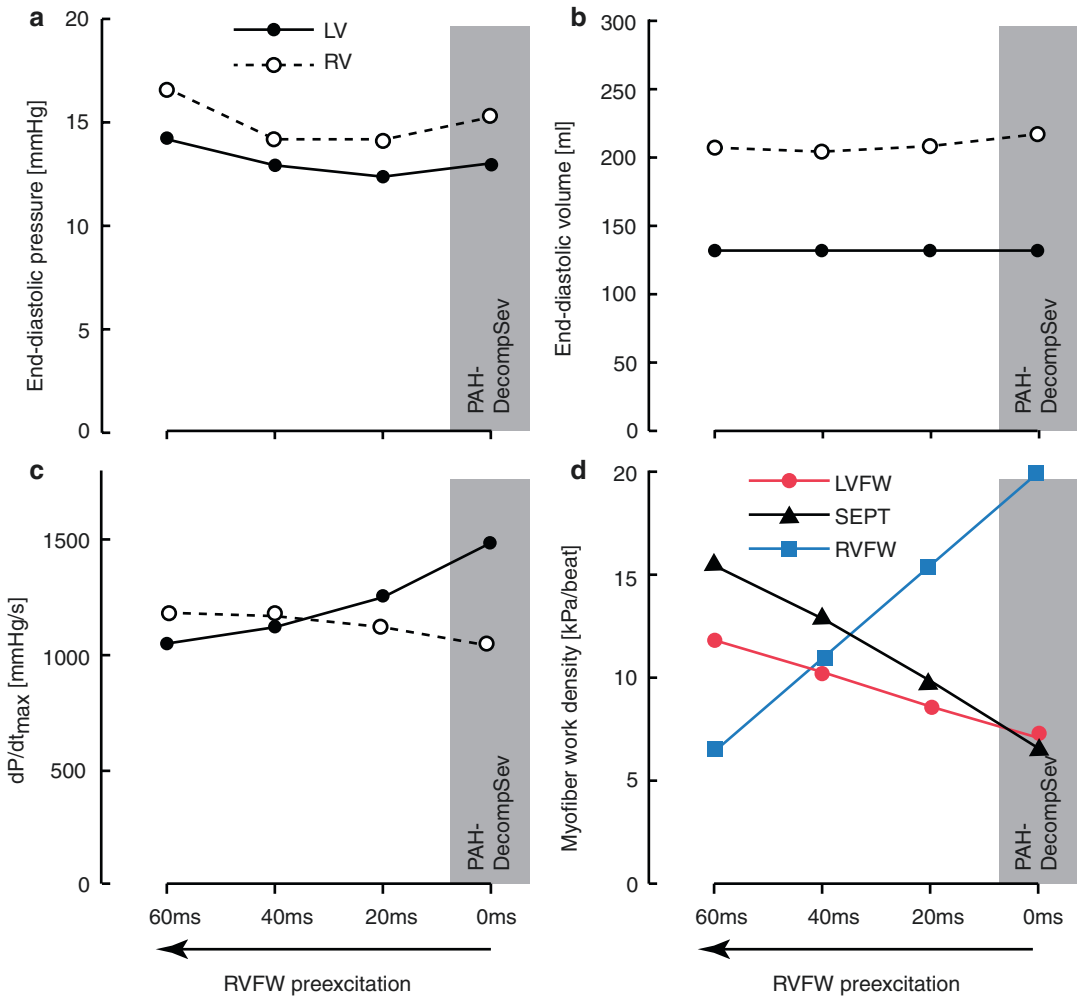


**Fig. 7.6** Simulated effect of right ventricular free wall (RVFW) pacing on cardiac pump function in severe PAH.  $dP/dt_{max}$  maximal rate of pressure rise, LV left ventricle, LVFW left ventricular free wall, RV right ventricle, SEPT

interventricular septum, RVFW right ventricular free wall, PAH-DecompSev severely decompensated PAH condition. Adapted from [32]

ventricular walls. Pre-excitation of the RV free wall resulted in more synchronous LV and RV pressure decay, more homogeneous distribution of myofiber load over the ventricular walls, and slight improvement of RV pump function. Pre-exciting the RV relieved the RV free wall from the extremely high myofiber work at the cost of an increase of myofiber work in the LV free wall and septum. The effects were maximal upon 40 ms pre-excitation of the RV free wall. The redistribution of myofiber work over the ventricular walls and the improvement in RV pump function

are apparently due to the mechanical interaction of the ventricular walls.

CircAdapt provided initial theoretical evidence that a therapeutic intervention such as RVFW pacing may improve RV pump function in decompensated PAH. Recent studies in isolated hearts of experimental animals with PAH [19] and in patients with severe chronic thromboembolic pulmonary hypertension [33] have subsequently demonstrated that RV pacing does indeed have beneficial effects on RV pump function.

## Conclusion and Future Perspectives

The CircAdapt model of the human heart and circulation produces realistic simulations of global hemodynamic pump function as well as of local mechanical deformation and work distribution in PAH. CircAdapt can be used to investigate *in silico* both the pathophysiological effects of PAH itself and its treatment on cardiac mechanics and hemodynamics. It is therefore a feasible platform to investigate new therapeutic strategies or to generate hypotheses on new therapies. Computer models like CircAdapt are likely to play an important role in the future in helping physicians to practice personalized, predictive and preventive medicine. By integrating the available clinical measurements in a multi-scale model of human cardiovascular dynamics, it is anticipated that the hemodynamic status of a patient can be estimated more precisely than by conventional means (i.e., based on individual measurements). We envision that earlier stages of disease are likely to become detectable, which in turn, may lead to better and more preventative medicine. It is interesting to speculate that patient-specific modeling may also reduce the inconvenience of regular monitoring to the patient and reduce direct healthcare costs. A more precise diagnosis, as well as the possibility of *in silico* testing of intended therapeutic interventions, will lead to more successful and efficient treatment of PAH patients, which may improve long-term prognosis and quality of life.

## References

1. Forfia PR, Vachieri JL. Echocardiography in pulmonary arterial hypertension. *Am J Cardiol.* 2012;110(6 Suppl):16S–24S.
2. Vonk-Noordegraaf A, Souza R. Cardiac magnetic resonance imaging: what can it add to our knowledge of the right ventricle in pulmonary arterial hypertension? *Am J Cardiol.* 2012;110(6 Suppl):25S–31S.
3. Chin KM, Coghlan G. Characterizing the right ventricle: advancing our knowledge. *Am J Cardiol.* 2012;110(6 Suppl):3S–8S.
4. Arts T, Delhaas T, Bovendeerd P, Verbeek X, Prinzen FW. Adaptation to mechanical load determines shape and properties of heart and circulation: the CircAdapt model. *Am J Physiol Heart Circ Physiol.* 2005;288(4):H1943–54.
5. Lumens J, Delhaas T, Kirn B, Arts T. Three-wall segment (TriSeg) model describing mechanics and hemodynamics of ventricular interaction. *Ann Biomed Eng.* 2009;37(11):2234–55.
6. Arts T, Lumens J, Kroon W, Delhaas T. Control of whole heart geometry by intramyocardial mechano-feedback: a model study. *PLoS Comput Biol.* 2012;8(2):e1002369.
7. Walmsley J, Arts T, Derval N, Bordachar P, Cochet H, Ploux S, et al. Fast simulation of mechanical heterogeneity in the electrically asynchronous heart using the multipatch module. *PLoS Comput Biol.* 2015;11(7):e1004284.
8. Belenkie I, Smith ER, Tyberg JV. Ventricular interaction: from bench to bedside. *Ann Med.* 2001;33(4):236–41.
9. Baker AE, Dani R, Smith ER, Tyberg JV, Belenkie I. Quantitative assessment of independent contributions of pericardium and septum to direct ventricular interaction. *Am J Phys.* 1998;275(2 Pt 2):H476–83.
10. Belenkie I, Sas R, Mitchell J, Smith ER, Tyberg JV. Opening the pericardium during pulmonary artery constriction improves cardiac function. *J Appl Physiol* (1985). 2004;96(3):917–22.
11. Omens JH. Stress and strain as regulators of myocardial growth. *Prog Biophys Mol Biol.* 1998;69(2–3):559–72.
12. Russell B, Curtis MW, Koshman YE, Samarel AM. Mechanical stress-induced sarcomere assembly for cardiac muscle growth in length and width. *J Mol Cell Cardiol.* 2010;48(5):817–23.
13. Olivetti G, Ricci R, Lagrasta C, Maniga E, Sonnenblick EH, Anversa P. Cellular basis of wall remodeling in long-term pressure overload-induced right ventricular hypertrophy in rats. *Circ Res.* 1988;63(3):648–57.
14. Minami S, Onodera T, Okazaki F, Miyazaki H, Ohsawa S, Mochizuki S. Myocyte morphological characteristics differ between the phases of pulmonary hypertension-induced ventricular hypertrophy and failure. *Int Heart J.* 2006;47(4):629–37.
15. Hardziyenka M, Campian ME, de Bruin-Bon HA, Michel MC, Tan HL. Sequence of echocardiographic changes during development of right ventricular failure in rat. *J Am Soc Echocardiogr.* 2006;19(10):1272–9.
16. Voelkel NF, Quaipe RA, Leinwand LA, Barst RJ, McGoon MD, Meldrum DR, et al. Right ventricular function and failure: report of a National Heart, Lung, and Blood Institute working group on cellular and molecular mechanisms of right heart failure. *Circulation.* 2006;114(17):1883–91.
17. Tanaka H, Tei C, Nakao S, Tahara M, Sakurai S, Kashima T, et al. Diastolic bulging of the interventricular septum toward the left ventricle. An echocardiographic manifestation of negative interventricular pressure gradient between left and right ventricles during diastole. *Circulation.* 1980;62(3):558–63.
18. Mori S, Nakatani S, Kanzaki H, Yamagata K, Take Y, Matsuura Y, et al. Patterns of the interventricular septal motion can predict conditions of patients with

- pulmonary hypertension. *J Am Soc Echocardiogr.* 2008;21(4):386–93.
19. Keogh AM, Mayer E, Benza RL, Corris P, Darteville PG, Frost AE, et al. Interventional and surgical modalities of treatment in pulmonary hypertension. *J Am Coll Cardiol.* 2009;54(1 Suppl):S67–77.
  20. Kurzyna M, Dabrowski M, Bielecki D, Fijalkowska A, Pruszczyk P, Opolski G, et al. Atrial septostomy in treatment of end-stage right heart failure in patients with pulmonary hypertension. *Chest.* 2007;131(4):977–83.
  21. Zierer A, Melby SJ, Voeller RK, Moon MR. Interatrial shunt for chronic pulmonary hypertension: differential impact of low-flow vs. high-flow shunting. *Am J Physiol Heart Circ Physiol.* 2009;296(3):H639–44.
  22. Koeken Y, Kuijpers NH, Lumens J, Arts T, Delhaas T. Atrial septostomy benefits severe pulmonary hypertension patients by increase of left ventricular preload reserve. *Am J Physiol Heart Circ Physiol.* 2012;302(12):H2654–62.
  23. Micheletti A, Hislop AA, Lammers A, Bonhoeffer P, Derrick G, Rees P, et al. Role of atrial septostomy in the treatment of children with pulmonary arterial hypertension. *Heart.* 2006;92(7):969–72.
  24. Chin KM, Kim NH, Rubin LJ. The right ventricle in pulmonary hypertension. *Coron Artery Dis.* 2005;16(1):13–8.
  25. Sandoval J, Bauerle O, Palomar A, Gomez A, Martinez-Guerra ML, Beltran M, et al. Survival in primary pulmonary hypertension. Validation of a prognostic equation. *Circulation.* 1994;89(4):1733–44.
  26. Galie N, Hoeper MM, Humbert M, Torbicki A, Vachiery JL, Barbera JA, et al. Guidelines for the diagnosis and treatment of pulmonary hypertension: the Task Force for the Diagnosis and Treatment of Pulmonary Hypertension of the European Society of Cardiology (ESC) and the European Respiratory Society (ERS), endorsed by the International Society of Heart and Lung Transplantation (ISHLT). *Eur Heart J.* 2009;30(20):2493–537.
  27. Bossone E, Avelar E, Bach DS, Gillespie B, Rubenfire M, Armstrong WF. Diagnostic value of resting tricuspid regurgitation velocity and right ventricular ejection flow parameters for the detection of exercise induced pulmonary arterial hypertension. *Int J Card Imaging.* 2000;16(6):429–36.
  28. Marcus JT, Gan CT, Zwanenburg JJ, Boonstra A, Allaart CP, Gotte MJ, et al. Interventricular mechanical asynchrony in pulmonary arterial hypertension: left-to-right delay in peak shortening is related to right ventricular overload and left ventricular underfilling. *J Am Coll Cardiol.* 2008;51(7):750–7.
  29. Beyar R. Heart inefficiency in pulmonary hypertension: a double jeopardy. *J Am Coll Cardiol.* 2008;51(7):758–9.
  30. Delhaas T, Arts T, Prinzen FW, Reneman RS. Regional fibre stress-fibre strain area as an estimate of regional blood flow and oxygen demand in the canine heart. *J Physiol.* 1994;477(Pt 3):481–96.
  31. Prinzen FW, Hunter WC, Wyman BT, McVeigh ER. Mapping of regional myocardial strain and work during ventricular pacing: experimental study using magnetic resonance imaging tagging. *J Am Coll Cardiol.* 1999;33(6):1735–42.
  32. Lumens J, Arts T, Broers B, Boomars KA, van Paassen P, Prinzen FW, et al. Right ventricular free wall pacing improves cardiac pump function in severe pulmonary arterial hypertension: a computer simulation analysis. *Am J Physiol Heart Circ Physiol.* 2009;297(6):H2196–205.
  33. Hardziyenka M, Surie S, de Groot JR, de Bruin-Bon HA, Knops RE, Rimmelink M, et al. Right ventricular pacing improves haemodynamics in right ventricular failure from pressure overload: an open observational proof-of-principle study in patients with chronic thromboembolic pulmonary hypertension. *Europace.* 2011;13(12):1753–9.